Influence of active mitigation barriers on LNG dispersion

Marsegan C., Busini V.*, Rota R.
Politecnico di Milano
Piazza Leonardo da Vinci 32
Department of Chemistry, Materials and Chemical Engineering "G. Natta"
*valentina.busini@polimi.it

Abstract

In recent years, particular interest has been direct to the issues of risk associated with the storage, transport and use of Liquefied Natural Gas (LNG) due to the increasing consideration that it is receiving for energy applications. Consequently, a series of experimental and modeling studies to analyze the behavior of LNG have been carried out to collect an archive of evaporation, dispersion and combustion information, and several mathematical models have been developed to represent LNG dispersion in realistic environments and to design mitigation barriers.
This work uses Computational Fluid Dynamics codes to model the dispersion of a dense gas in the atmosphere after accidental release. In particular, it will study the dispersion of LNG due to accidental breakages of a pipeline and it will analyze how it is possible to mitigate the dispersing cloud through walls and curtains of water vapor and air, also providing a criterion for the design of such curtains.

Keywords
Liquefied Natural Gas (LNG); mitigation barriers; heavy gas dispersion; obstacles; vapor curtains; safety

1 Introduction

In the past years, interest has increased in the issues of risk associated with the storage, transport and use of LNG due to the increasing consideration that it is receiving for energy applications. A series of experimental and modeling studies to analyze the behavior of LNG have been carried out to collect an archive of evaporation, dispersion and combustion information (Britter & Griffiths, 1982; Ermak, Chan, Morgan, & Morris, 1982; Koopman et al., 1982; Luketa-Hanlin, 2006; Puttock, Blackmore, & Colenbrander, 1982). Based on this information, several modeling based works have been developed to represent LNG dispersion in realistic environments (Blocken, van der Hout, Dekker, & Weiler, 2015; Koopman & Ermak, 2007; Koopman, Ermak, & Chan, 1989; Luketa-Hanlin, Koopman, & Ermak, 2007; Schleder, Pastor, Planas, & Martins, 2015; Zhang, Li, Zhu, & Qiu, 2015); these models can be used both to estimate the hazardous area in case of an accidental release of LNG, as well as to investigate the efficiency of potential mitigation measures (Busini, Lino, & Rota, 2012; Busini & Rota, 2014; Derudi, Bovolenta, Busini, & Rota, 2014; Kim, Mentzer, & Mannan, 2014).
Recently, the effect of mitigation barriers with different shapes has been investigated, resulting in the conclusion that passive barriers act only as a physical hindrance without enhancing the mixing rate between cloud and air due to the remarkable inertia of large LNG releases (Busini & Rota, 2014). Other works, based on experimental tests or modeling, support the idea that forced dispersion is more appropriate for diluting hazardous gas clouds, suggesting the use of spray curtains (Bara & Dusserre, 1997; Buchlin, 1994; Diaz-Ovalle, Vazquez-Roman, Lesso-Arroyo, & Mannan, 2012; Rana, Cormier, Suardin, Mang, & Mannan, 2008; Rana, Guo, & Mannan, 2010).
The purpose of this work was to analyze, through a Computational Fluid Dynamics (CFD) model, the dispersion of a dense gas, namely LNG, to provide a criterion for designing an active barrier (i.e. a barrier releasing some fluid within the cloud) that can dilute the cloud below the lower

flammability limit (LFL). It should be noted that, in this work, the presented methodology was applied to the LFL as threshold for flammable vapor dispersion distances, but the same methodology can be applied to the 50% of the LFL threshold.

2 Material & Methods

The commercial package Fluent 12.1.2 (ANSYS Inc., 2009) was used for all the computations, together with the boundary conditions summarized in Table 1. The k–ε model complemented with the Atmospheric Stability sub-Model (ASsM) (Pontiggia, Derudi, Busini, & Rota, 2009) was used for representing the effects of the turbulence.

Table 1 Boundary conditions.

Ground	Wall @ 298 K, roughness = 0.01 m
Walls	Adiabatic wall, roughness = 0.01 m
Pool	During atmospheric stabilization: Wall @ 298 K, roughness = 0.01 m
	During pool evaporation: Mass flow inlet
	After the end of pool evaporation: Adiabatic wall
Wind inlet, domain sides, sky	Velocity inlet
Wind outlet	Pressure outlet

3 Proposed methodology

Since one of the main characteristics of cold and dense clouds is their ability of reducing turbulence thus reducing the effects of terrain and obstacles (Businі & Rota, 2014; Koopman, et al., 1989), in this work the efficiency of active mitigation barriers, designed with the aim of diluting the dense gas cloud through jets of steam or air, was investigated.

The methodology used to define the characteristics of an active mitigation barrier necessary to stop cloud dispersion is sketched in the flow diagram in Figure 1 and discussed later on. It should be noted that before starting the procedure a maximum allowed hazardous distance should be defined: that is, the maximum distance from the source at which the concentration of the cloud can reach the LFL value (X_{cld_max}), and a maximum mitigation wall height both in terms of executive/structural and visual impression (h_{obs_max}).

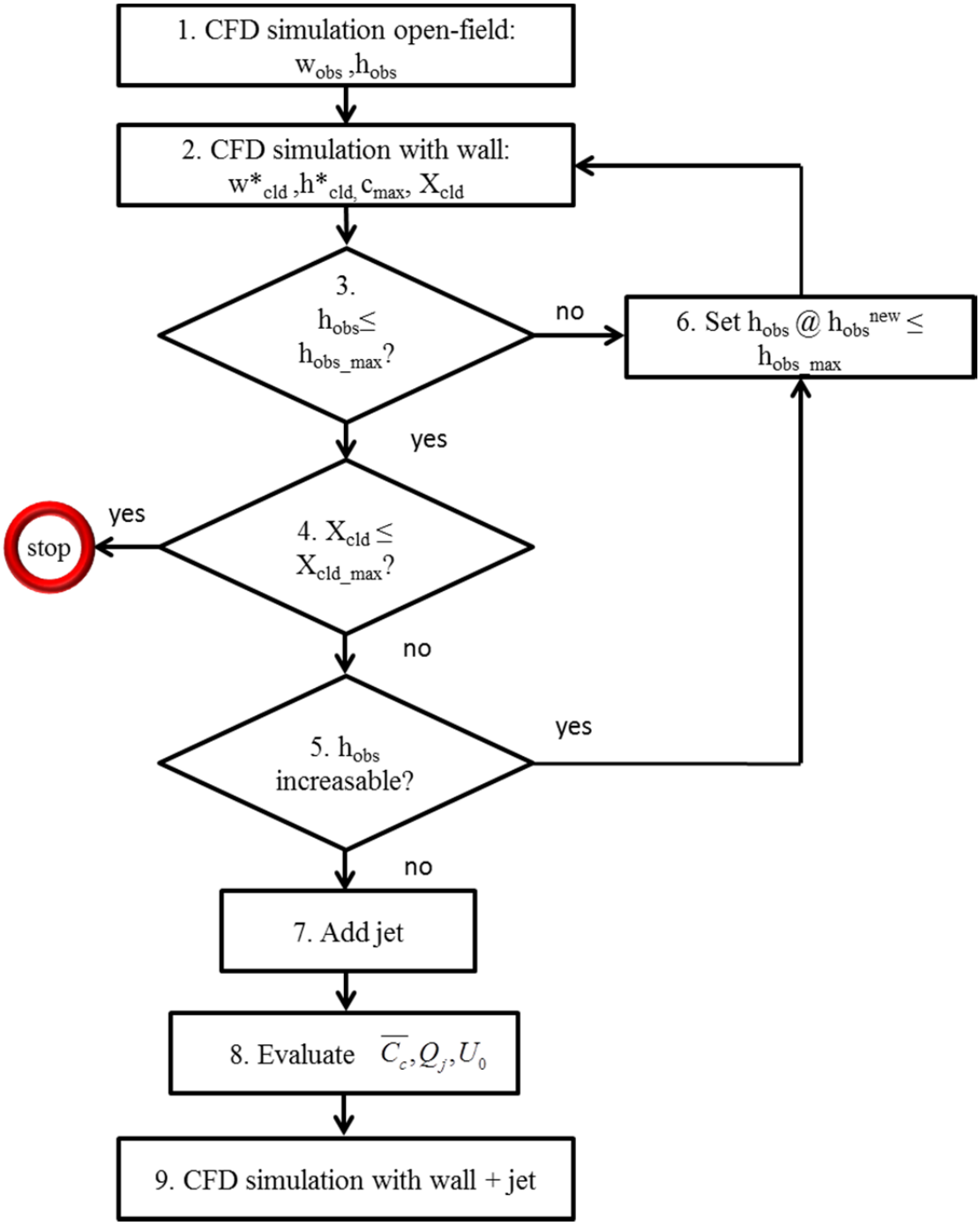

Figure 1 Flow diagram of the proposed methodology; h_{obs} and w_{obs}: minimum dimensions of the mitigation wall, w^*_{cld} and h^*_{cld}: cloud width and height at the mitigation wall distance, X_{cld_max} maximum distance from the source at which cloud concentration can reach the LFL value, h_{obs_max} maximum mitigation wall height, C_{max} maximum cloud concentration in correspondence with the wall position, the top-hat concentration, hypothesizing a Gaussian distribution, Q_j: the flow rate of the jet, U_0: initial jet velocity.

The first step of the methodology is the simulation, using a suitable CFD model, of open-field cloud dispersion, that is in the actual environment in which the release takes place without any mitigation barriers, which allows the definition of the minimum dimensions (h_{obs} and w_{obs}) of the mitigation wall that can stop cloud dispersion according to the procedure discussed in detail elsewhere(Busini, et al., 2012; Busini & Rota, 2014; Derudi, et al., 2014).

Such a procedure is based on the definition of a dimensionless parameter involving the ratio between the height of the frontal face of a given obstacle, h_{obs} (or the width w_{obs}), and the cloud height h_{cld} (or cloud width w_{cld}) evaluated in open field conditions at the same distance from the source:

$$R^* = \min\left(\frac{h_{obs}}{h_{cld}}, \frac{w_{obs}}{w_{cld}}\right) \qquad (1)$$

It has been found that for values of $R^* \geq 1$ the obstacles influence cloud dispersion and could even block it completely (Derudi, et al., 2014).

The second step of the procedure requires a simulation of cloud dispersion in the presence of a passive mitigation barrier with R^*=1. This simulation makes it possible to compute the cloud width (w^*_{cld}) and height (h^*_{cld}) at the mitigation wall distance, as well as its maximum concentration in correspondence with the wall position (C_{max}) and the maximum hazardous distance from the source where the concentration is equal to the LFL (X_{cld}). At this point different scenarios open:

A. the wall has a reasonable height (step 3) and the hazardous distance is acceptable (step 4): the process can be considered concluded since a passive barrier is able to stop the cloud;
B. the wall height is higher than the h_{obs_max} and a new simulation with h_{obs} fixed at h_{obs_max} has to be performed:
    a. if the hazardous distance is acceptable (step 4): the process can be considered concluded since a passive barrier is able to stop the cloud;
    b. if the hazardous distance is not acceptable (step 4), considering that h_{obs} is at its maximum value: a jet can be added to the top of the wall (step 7) (sometimes this can lead also to a lowering of the wall height, as will be described further on);
C. the wall has a reasonable height (step 3) but the hazardous distance is not acceptable (step 4):
    a. if h_{obs} is increasable, a new simulation with a new higher wall can be performed (that is, go back to step 2);
    b. if h_{obs} is not increasable: a jet can be added to the top of the wall (step 7) (sometimes this can lead also to a lowering of the wall height, as will be described further on);

In case an active barrier is necessary (step 7), the following step 8 involves the definition of the jet flow rate. Assuming the jet rises from the top of the wall, three flows converge above the wall as shown in Figure 2: Q_c, Q_j, and Q_a, which are the flow rate of the cloud, of the jet, and of the air entrainment downstream of the wall, respectively.

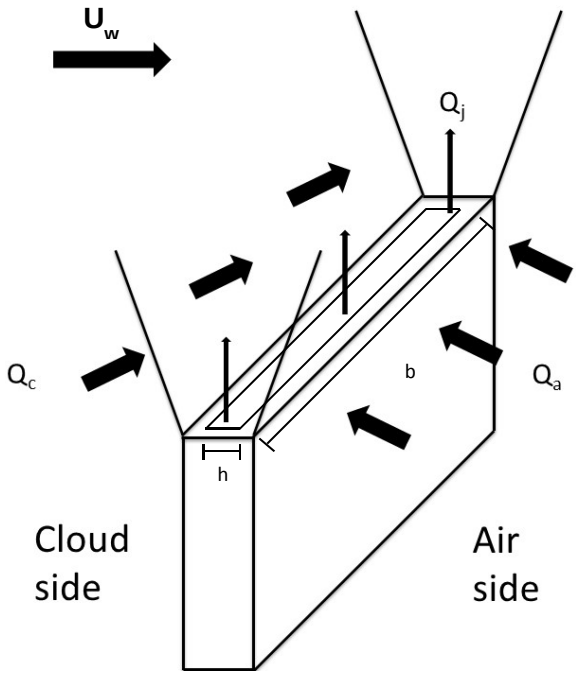

Figure 2 Flows confluent over the wall

The value of the total entrainment flow rate, Q_{ent}, depends on the type and flow rate of the jet. Considering an isothermal plane jet (namely a jet arising from a rectangular nozzle), the relation between Q_j (the jet flow rate) and Q_{ent} is the following (Awbi, 1991; Rajaratnam, 1976):

$$Q_{ent}(x) = 0.31 \cdot Q_j \cdot \sqrt{\frac{x}{h}} \qquad (2)$$

where x is the distance from the jet nozzle and h is the width of the rectangular nozzle.
The relationship between the initial jet velocity, U_0, and the centerline velocity at a distance x from the nozzle, U_m, is the following (Rajaratnam, 1976):

$$U_m(x) = U_0 \cdot \frac{2.47}{\sqrt{x/h}} \qquad (3)$$

and:

$$Q_{ent}(x) = 0.76 \cdot Q_j \cdot \frac{U_0}{U_m} \qquad (4)$$

From this last equation we can estimate the jet entrainment from the "air side" of the mitigation barriers as (see figure 2):

$$Q_a(x) = \frac{1}{2} Q_{ent}(x) = 0.38 \cdot Q_j \cdot \frac{U_0}{U_m} \qquad (5)$$

The jet entrainment from the "cloud side" of the mitigation barrier can be estimated assuming that the jet is able to entrain all the cloud flow rate that hits the mitigation barrier. With this assumption, Q_c is evaluated from the wind velocity (U_w) and the cloud width (w^*_{cloud}) and height (h^*_{cloud}) overcoming the mitigation barrier. These last values are obtained from the CFD simulation carried

out in step 2 of the previously discussed flow diagram (see figure 1) and allows Q_c to be computed as:

$$Q_c = w^*_{cld} \cdot h^*_{cld} \cdot U_w \qquad (6)$$

From the aforementioned CFD simulations, the maximum concentration of the cloud in correspondence to the wall position (C_{max}) can be evaluated: a monitor panel that records the maximum concentration value throughout the whole simulation at every output time step (1 second) should be placed along the centerline of the wall, as wide as the wall itself and as high as the total domain. Consequently, is it also possible to calculate the equivalent top-hat concentration ($\overline{C_c}$), hypothesizing a Gaussian distribution in the cloud in correspondence to the wall (Figure 3) and requiring that the area under the Gaussian curve be equal to the area of a rectangle of height $\overline{C_c}$ and width $2y_c$ according to equation 7:

$$\int_{-y_c}^{y_c} \frac{const}{\sigma_y\sqrt{2\pi}} exp\left(-\frac{y^2}{2{\sigma_y}^2}\right) dy = 2 \cdot \overline{C_c} \cdot y_c \qquad (7)$$

where $\pm y_c$ are the cloud half-widths in correspondence to the LFL value (computed from the CFD simulation in correspondence to the wall), as shown in Figure 3. The value of the constant can be obtained from the boundary condition:

$$C(y = 0) = \frac{const}{\sigma_y\sqrt{2\pi}} = C_{max} \qquad (8)$$

and the value of σ_y from the relation:

$$\sigma_y = \frac{y_c}{\sqrt{2ln\frac{C_{max}}{LFL}}} \qquad (9)$$

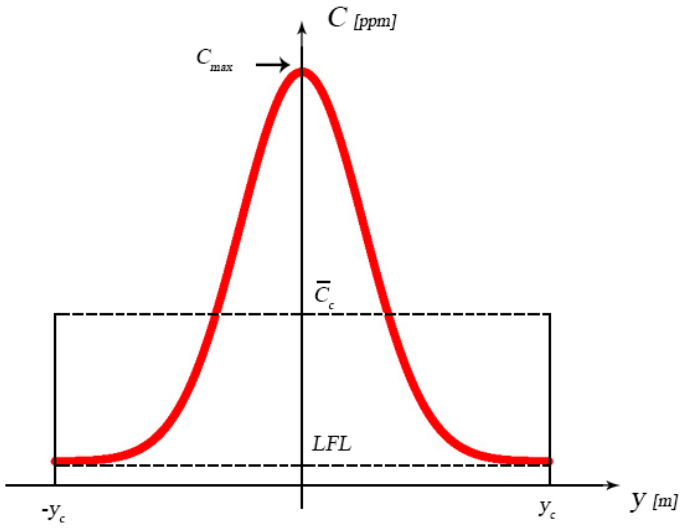

Figure 3 Gaussian distribution and mean concentration definition.

After solving equation 7, the average concentration $\overline{C_c}$ can be conveniently expressed as a function of the LFL value as follows:

$$\overline{C_c} = \alpha \cdot LFL \qquad (10)$$

The total mass flow rate (Q_{tot}), which is the sum of Q_c, Q_a, and Q_j, should dilute the cloud concentration at least to the LFL, which means:

$$\frac{Q_c \cdot \overline{C_c}}{Q_c + Q_j + Q_a} = \frac{Q_c \cdot \alpha \cdot LFL}{Q_{tot}} \leq LFL \qquad (11)$$

For the minimum dilution requirement this relation becomes:

$$Q_{tot} = Q_c \cdot \alpha \qquad (12)$$

Using the previous relations for Q_c and Q_a, the following relation for Q_{tot} can be obtained:

$$Q_{tot} = Q_c + Q_j + Q_a = w^*_{cld} \cdot h^*_{cld} \cdot U_w + Q_j + 0.38 \cdot Q_j \cdot \frac{U_0}{U_m(x)} \qquad (13)$$

Under the hypothesis that the jet exhausts its mitigation action when its velocity ($U_m(x)$) is equal to that of the wind (U_w), this equation results in the following one:

$$Q_{tot} = w^*_{cld} \cdot h^*_{cld} \cdot U_w + Q_j \cdot \left(1 + 0.38 \cdot \frac{U_0}{U_w}\right) \qquad (14)$$

Q_j and U_0 are related to each other since:

$$Q_j = A_j \cdot U_0 = b \cdot h \cdot U_0 \qquad (15)$$

with b and h respectively being the length and width of the jet nozzle as shown in Figure 2.
From these equations, the following relation can be deduced:

$$\alpha \cdot w^*_{cld} \cdot h^*_{cld} \cdot U_w = w^*_{cld} \cdot h^*_{cld} \cdot U_w + Q_j \cdot \left(1 + 0.38 \cdot \frac{Q_j / b \cdot h}{U_w}\right) \qquad (16)$$

from which the only unknown, Q_j, can be easily computed as:

$$Q_j = \frac{-1 + \sqrt{1 - 4 \cdot \beta \cdot (1 - \alpha) \cdot Q_c}}{2 \cdot \beta} \qquad (17)$$

where $= \frac{0.38}{b \cdot h \cdot U_v}$, $\alpha = \frac{\overline{C_c}}{LFL}$, and $Q_c = w^*_{cld} \cdot h^*_{cld} \cdot U_w$.

4 Results

4.1 First case study: massive release of LNG

As a first case study, a release of LNG deriving from the full-bore rupture of a pipeline was selected. The characteristics of both pipeline and storage are reported in Table 2.

Table 2 Characteristics of both pipeline and storage.

Pipeline diameter	1 m
Total inventory	45,000 kg
Temperature	111 K
Pipeline length	20 m
Density	450 kg/m3

Using the suite package PHAST 6.42 (DNV, 1999), the modeling of the LNG dispersion was performed for a neutral stability class and 5 m/s wind speed at 10 m above the ground (5D) in order to define the pool dimension deriving from the spill and the evaporating mass flow; the maximum distance reached by the LFL contour predicted by the integral model was about 570 m from the center of the pool. These results are expected to be reliable in the absence of large obstacles, since PHAST has been successfully validated for comparison with experimental open field (DNV, 1999) data.
The source term estimated using PHAST and shown in Figure 4 was used in the CFD simulations considering a pool with a radius of 10 m and a mesh built using GAMBIT (ANSYS Inc., 2004) size functions to make the grid denser in the critical areas; the size of the domain of integration was 800x1000x50 m^3.

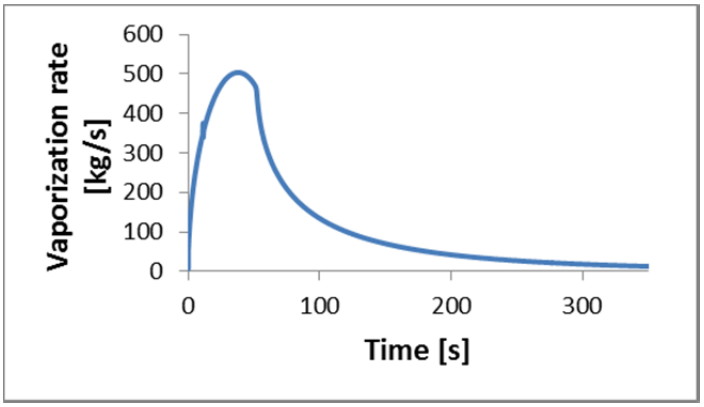

Figure 4 - Source term computed with PHAST and used in the CFD simulations.

A comparison of the CFD results in open field conditions with those of the integral model is shown in Figure 5a in terms of LFL footprint; we can see that, as expected, the two approaches give similar results in open field conditions. The grid independence analysis is also summarized in Figure 5a and 5b: we can see that the results of the medium mesh ($1.80 \cdot 10^6$ cells) are comparable with those of the most dense one ($1.48 \cdot 10^7$ cells), therefore the former was used as a base for the successive meshes.

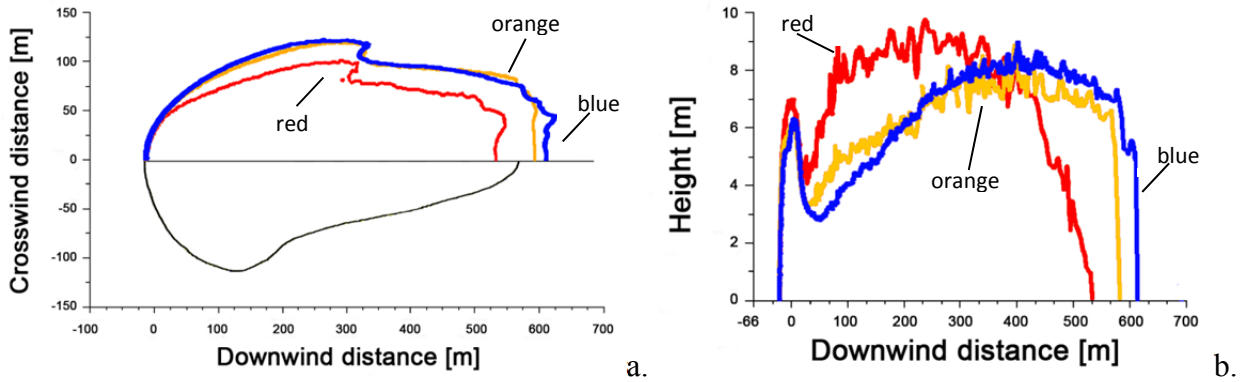

Figure 5 Maximum LFL footprint in open field conditions (a): the upper part reports the CFD model predictions obtained with $4 \cdot 10^5$ cells (red line), $1.80 \cdot 10^6$ cells (orange line), and $1.48 \cdot 10^7$ cells (blue line); the bottom part reports predictions of the integral model. (b): cloud height profile at LFL along the wind direction in correspondence with the domain symmetry plane, predicted by the CFD model (color code as in part a).

The boundary conditions of the pool surface, initially set as *wall* with the same characteristic of the terrain (during the first phase of wind stabilization), was changed to *mass flow inlet* and then switched to *adiabatic walls* at the end of pool evaporation.

In accordance with the criterion of R^*=1, a mitigation barrier at 150 m downwind the pool center should be about 6 m high (see Figure 5b); it is expected that adding a passive barrier will spread the dense gas cloud in the proximity of the barrier in the crosswind direction, therefore the ratio $\frac{w_{obs}}{w_{cld}}$ was chosen to be equal to 2, in order to thoroughly contain the entire width of the cloud. The passive barrier was therefore designed to be 450 m wide. More details on the effect of the barrier width can be found elsewhere (Derudi, et al., 2014).

It is worth mentioning that since a mitigation barrier is expected to protect a sensitive target close to the plant, this leads usually to locate the barrier in between the source and the target. In this framework, only downwind locations of the mitigation barriers have been considered in this work. Of course, other wind directions could lead to a strong reduction of the barrier efficiency, in particular when the wind drives the cloud outside the barrier width; however, in this case the sensitive target would not be downwind the source.

The simulation performed with the passive mitigation barrier resulted in the cloud dispersion sketched in Figure 6.

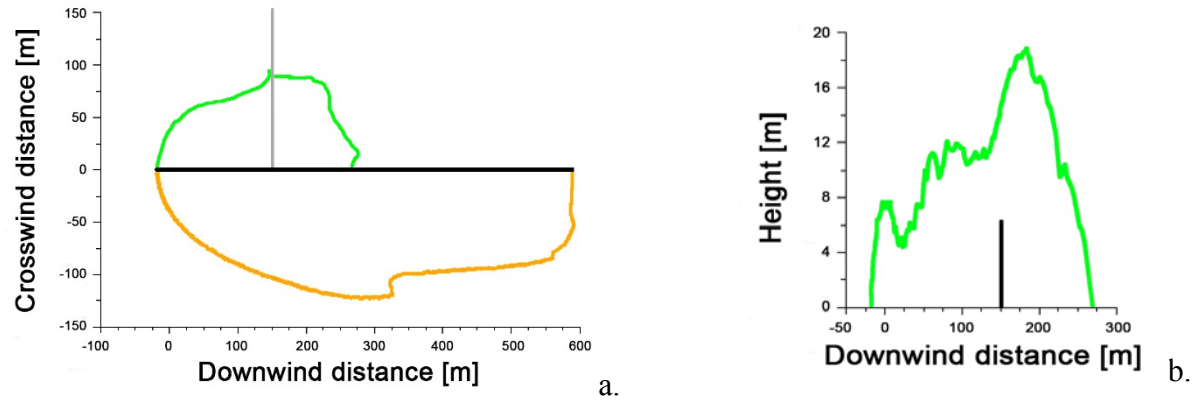

Figure 6 a) Maximum LFL footprint in the presence of the passive mitigation barrier (upper part) and in open field conditions (lower part); b) Cloud height profile at LFL along the wind direction, in correspondence with the domain symmetry plane, predicted by the CFD model in the presence of a mitigation barrier.

The passive mitigation barrier acts as a physical barrier to the LNG cloud: it does not bypass the wall laterally, and the maximum extension of the LFL profile in the wind direction reaches 280 m away from the center of the pool, which is about half the value obtained in open-field conditions.
From this simulation it is possible to evaluate h^*_{cloud}, w^*_{cloud} and C_{max} (step 2 of the procedure outlined in Figure 1). Assuming that the hazardous distance would not be acceptable, from these values we can compute the jet mass flow Q_j value and proceed through steps 7-8-9. The main data computed are summarized in Table 3:

Table 3 Main parameters computed using the proposed procedure

h^*_c	6 m
$w^*_c=2\cdot y_c$	180 m
C_{max}	150000 ppm
h	0.14 m
b	260 m
Q_c	7650 m^3/s
$\overline{C}_c$	106000 ppm
Q_{tot}	18437 m^3/s
Q_j	2046 m^3/s
U_0	56 m/s

4.2 Active mitigation barriers with vertical steam jet

The jet velocity necessary to dilute the cloud to the LFL value computed in the previous section was used to perform a simulation with a steam jet, released vertically from the top of the barrier at a temperature equal to 573 K. Moreover, other simulations with a steam jet velocity of 20, 30, 45 and 80 m/s respectively were performed to evaluate the sensitivity of the hazardous distance to the jet velocity. In all the simulations, the steam jet was activated after 35 s from the beginning of pool evaporation, that is when the cloud reaches the active mitigation barrier.
The results of these simulations are summarized in Figure 7 in terms of LFL footprint. The results obtained with the passive barrier are also reported for the sake of comparison. These results show that when the jet velocity is lower than that calculated with the proposed procedure, the steam jet is not able to dilute the cloud under the LFL, and so the hazardous distance does not change significantly with respect to the passive barrier even if the hazardous area downwind of the barrier is significantly lower.

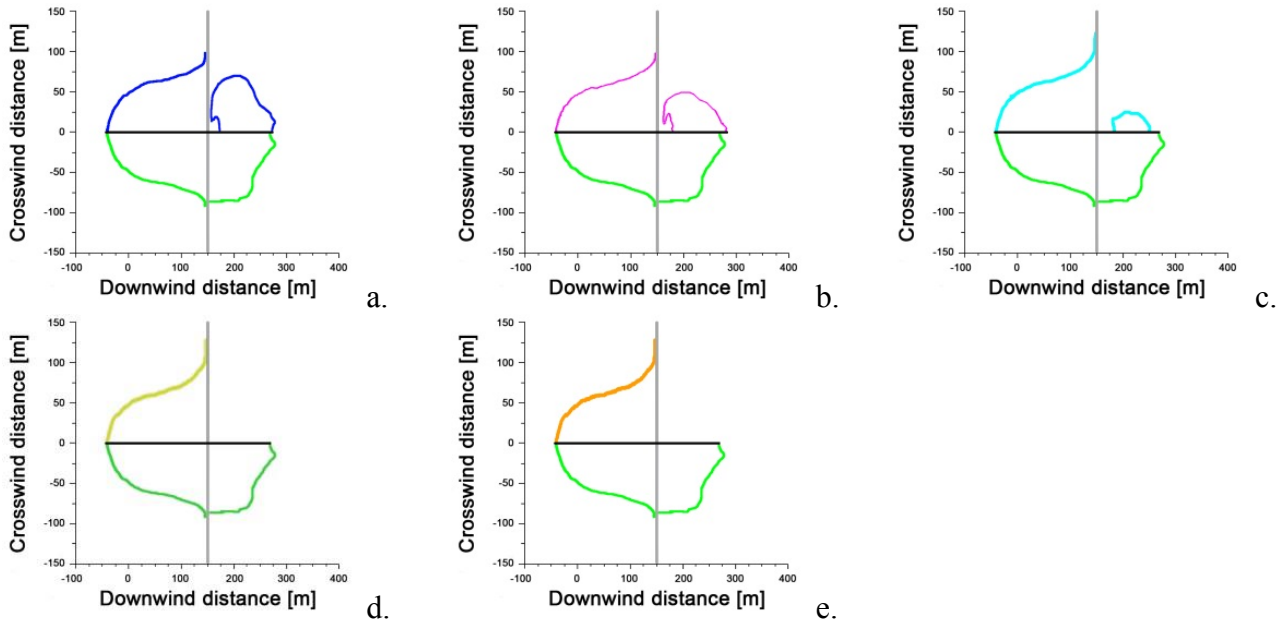

Figure 7 Upper part: maximum LFL footprint in the presence of active mitigation barriers (6 m wall with 573 K steam jet) for U_0 equal to 20 m/s (a), 30 m/s (b), 45 m/s (c), 56 m/s (d), and 80 m/s (e); lower part: maximum LFL footprint in the presence of a passive mitigation barrier (6 m wall).

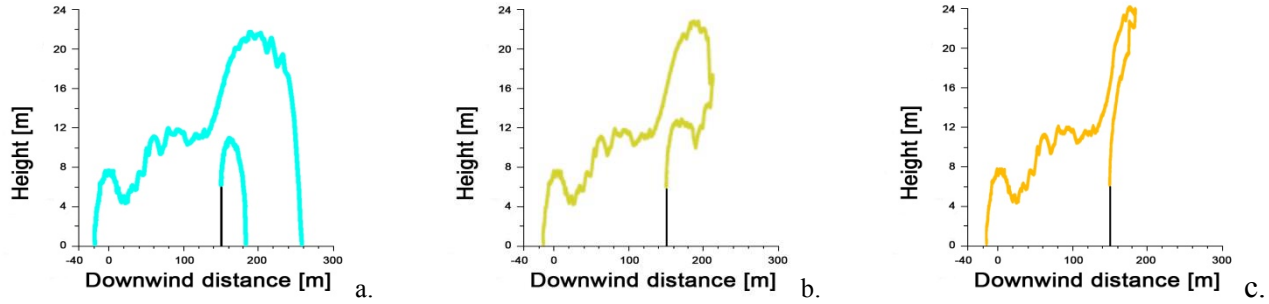

Figure 8 Cloud height profile at the LFL in the presence of active mitigation barriers (6 m wall with 573 K steam jet) with U_0 equal to 45 m/s (a), 56 m/s (b), and 80 m/s (c).

These results can be understood by looking at the cloud profiles at the LFL shown in Figure 8, where it can be seen that for jet velocities equal to or larger than the value required to dilute the cloud up to the LFL, the jet entrains both the cloud and the fresh air and rapidly mixes them, preventing LNG downwash to the ground. However, lower values of jet velocity do not take the cloud below the LFL. Therefore the LNG cloud at first rises due to the jet momentum, but rapidly falls due to its lower temperature. This means that the heating effect of the hot jet is quite negligible and the main effect of the active barrier is related to cloud dilution and mixing.

Figure 8 shows also that the presence of the jet on the wall top act like elevating the wall itself, therefore the wall height is maintained at a reasonable value.

Table 4 summarizes all the results in terms of the hazardous distance reached by the cloud beyond the barrier with respect to the base case (vertical passive barrier) and with respect to the open field condition.

4.3 Active mitigation barriers with inclined steam jet

In a previous work it has been shown that tilted passive barriers work better than straight ones (Busini & Rota, 2014), therefore, the efficacy of an inclined jet upwind of 45° was investigated. The steam was released at 45 m/s and the result sketched in Figure 9 shows that no differences are appreciable with respect to the case with vertical jet as sketched in Figure 7c.

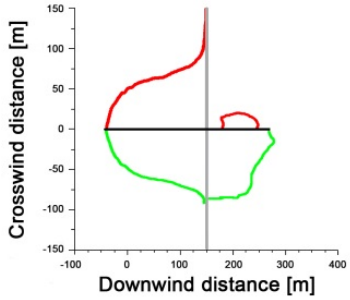

Figure 9 Upper part: downwind distance reached by the LFL in the configuration with the 6 m wall with 573 K steam jet with U_0= 45 m/s and inclined upwind of 45°; lower part: downwind distance reached by the LFL in the configuration with the 6 m wall without steam jet.

4.4 Tilted active mitigation barriers with steam jet

The behavior of a simple tilted passive mitigation barrier, overall height 6 m, characterized by a first straight part 4 m high and a top part inclined upwind with an angle of 45° from the vertical, was investigated. The results, in terms of the LFL footprint, are summarized in Figure 10a: in this case the influence of the tilted passive barrier on cloud dispersion is comparable with the simple wall (see also Table 4). On the other hand, the presence on the tilted upper part of a steam jet with an initial velocity of 45 m/s can stop cloud dispersion, as shown in Figure 10b. It is worth mentioning that the inclined top part of the mitigation barrier allows for a smaller steam velocity in order to stop the cloud with respect to the vertical wall (namely, 45 m/s vs. 56 m/s).

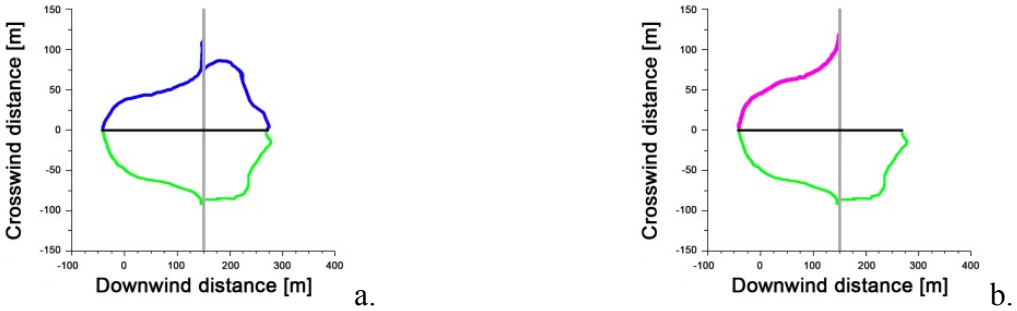

Figure 10 Upper part: downwind distance reached by the LFL in the configuration with the tilted 6 m wall without the steam jet (a) and with 573 K steam jet with U_0= 45 m/s (b). Lower part of both the figures: downwind distance reached by the LFL in the configuration with the 6 m wall without steam jet.

4.5 Tilted active mitigation barriers with air jet

From the previous simulations it seems that the high temperature of the steam does not significantly affect cloud dispersion by warming the cold LNG release. This assumption was verified by repeating the best configuration, in terms of steam requirement (that is, the tilted active mitigation barrier-see Figure 10b), using an air jet at ambient temperature with different velocities. Figure 11c reports the results of such a simulation, to be compared with the results summarized in Figure 10b for the steam jet. The efficacy of the air jet is the same as that of the steam jet; moreover, Figure 11 also reports the results for tilted active mitigation barriers with lower air jet velocity, namely 20 and 30 m/s showing that with the tilted wall, the jet velocity can be further decreased up to 30 m/s (which is about 50% of the estimated value for a vertical plane jet).

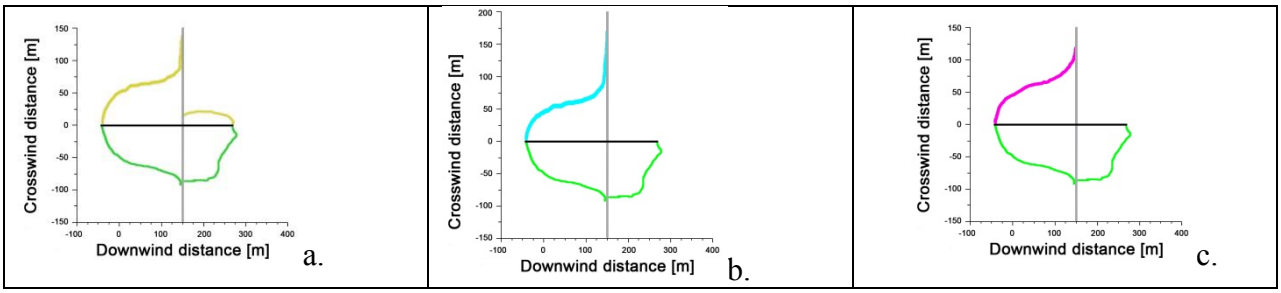

Figure 11 Upper part: maximum LFL footprint in the presence of active mitigation barriers (6 m wall with air jet) for U_0 equal to 20 m/s (a), 30 m/s (b), 45 m/s (c); lower part: maximum LFL footprint in the presence of a passive mitigation barrier (6 m wall).

Table 4. Mitigation effectiveness of the various investigated barriers (massive release scenario).

Barrier		Downwind distance (from the barrier position) reached by LFL [m]	Variation (with respect to the vertical passive barrier) of the LFL distance from the barrier position	Downwind distance (from the pool center) reached by LFL [m]	Variation (with respect to the open-field) of the LFL distance from the pool center
Vertical	Passive	130	-	280	-52%
	Active with vertical steam jet @ 20 m/s	130	0%	280	-52%
	Active with vertical steam jet @ 30 m/s	130	0%	280	-52%
	Active with vertical steam jet @ 45 m/s	108	-27%	258	-56%
	Active with vertical steam jet @ 56 m/s	0	-100%	150	-75%
	Active with vertical steam jet @ 80 m/s	0	-100%	150	-75%
	Active with vertical steam jet 45° @ 45 m/s	108	-27%	258	-56%
Tilted	Passive	128	-2%	278	-53%
	Active with steam jet @ 45 m/s	0	-100%	150	-75%
	Active with air jet @ 20 m/s	130	0%	280	-52%
	Active with air jet @ 30 m/s	0	-100%	150	-75%
	Active with air jet @ 45 m/s	0	-100%	150	-75%

4.6 Second case study: leakage of LNG

As a second case study, a leak from a pipeline of LNG was investigated.
The characteristics of the simulated scenario are reported in Table 5.

Table 5 Characteristics of the leak scenario.

Pipeline Diameter	1 m
Hole diameter	20% of the pipe
Mass discharged	11,250 kg
Temperature	111 K
Pump head	8 bar

As for the first case study, the modeling of the LNG dispersion was performed for a neutral stability class and 5 m/s wind speed at 10 m above the ground (5D) with the suite package PHAST 6.42 (DNV, 1999), in order to define the pool dimension deriving from the spill and the evaporating mass flow. The evaluated source term was used in the CFD simulations considering a pool with an average radius of 6 m and a mesh built using GAMBIT (ANSYS Inc. 2004) size functions to make the grid denser in the critical areas; the size of the domain of integration was reduced to 250x800x50 m^3 (with $2.3 \cdot 10^6$ cells), taking advantage of the reduced dimension of the cloud. Following the procedure discussed previously, the tilted 6 m wall, with a width of 300 m, was

positioned at 80 m from the pool center. The data reported in Table 6 were computed from the CFD simulation.

Table 6 Main parameters computed using the proposed procedure

h^*_{cloud}	3.5 m
$w^*_{cloud}=2 \cdot y_n$	110 m
C_{max}	155000 ppm
h	0.14 m
b	150 m
Q_n	1925 m^3/s
$\overline{C_n}$	108643 ppm
Q_{tot}	4754.75 m^3/s
Q_i	756 m^3/s
U_0	36 m/s

The application of the aforementioned methodology for estimating the air jet velocity resulted in U_0 = 36 m/s; considering that from the previous case with the tilted wall the necessary air velocity was half of that calculated, the simulation was performed with an air jet velocity of 18 m/s. As expected, due to both the lower size of the jet slot and the lower jet velocity, the required flow rate is more reasonable than that of the previous accidental scenario.
The results are sketched in Figure 12 and in Table 7.

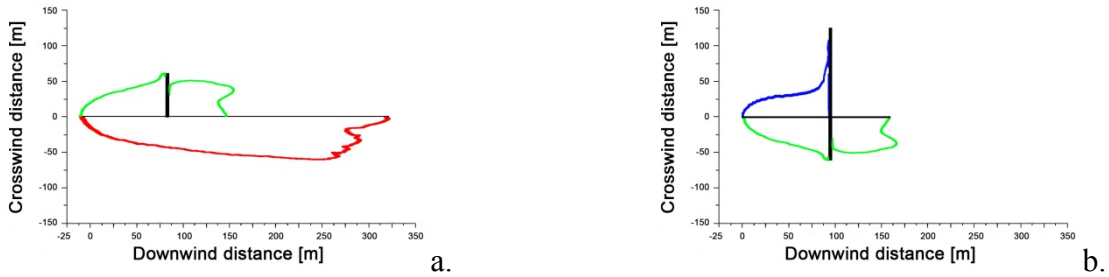

Figure 12 (a) upper part: downwind distance reached by the LFL with the tilted passive mitigation barrier; lower part: downwind distance reached by the LFL under open field conditions; (b) upper part: downwind distance reached by the LFL with the tilted active mitigation barrier (U_0 = 18 m/s); lower part: downwind distance reached by the LFL with the tilted passive mitigation barrier.

A passive mitigation barrier is not able to stop the cloud dispersion completely, while the active one can.

Table 7 Mitigation effectiveness of the various investigated barriers (leak scenario).

	Barrier	Downwind distance (from the barrier position) reached by LFL	Variation (with respect to the wall case) of the LFL distance from the barrier position	Downwind distance (from the pool center) reached by LFL [m]	Variation (with respect to the open-field) of the LFL distance from the pool center
'	Open field	-	-	325	-

Tilted	Passive	70 m	0%	150	-54%
	Active with air jet @ 30 m/s	0 m	-100%	80	-75%

5 Discussion

As presented in section 3, the proposed methodology mainly assumes that the jet above the barrier acts as a semi-permeable barrier, which rises and dilutes the cloud while mixing itself with the cloud. In other words, the jet is not able neither to increase significantly the cloud turbulence (in agreement with the findings of (Businì & Rota, 2014; Koopman, et al., 1989) , nor to reduce significantly the cloud density by heating it (since the enthalpy flow required to heat the cold gas cloud, up to make it neutral or even negatively buoyant, is very high).
The reasonableness of these assumptions has been confirmed by the simulations carried out and previously discussed. In particular, Figure 7 shows that the developed procedure is able to correctly predict the flow rate of the jet necessary to stop the cloud: for jet velocities lower than the value computed through the procedure, the active barrier is not able to stop completely the cloud, even if it can rise the cloud (see Figure 8, which clearly shows that the effectiveness of the active barrier is mainly linked to steric effects and mixing) and therefore reducing the impact of the accidental release behind the mitigation barrier (marginally in terms of hazardous distance, but more significantly in terms of impact area, see Figure 7).
Moreover, the substantial irrelevance of the jet temperature is evident from the results summarized in Figures 10b and 11c, where the effects of using steam jets at 573 K or air jets at 300 K are compared.
The enhancing effect of tilting the upper part of the barrier previously evidenced for passive barriers (Businì & Rota, 2014) has been confirmed also for active barriers, demonstrating that such a tilting allows reducing the required flow rate of almost 50% with respect to the value calculated by the proposed methodology (see Figure 11b and 12b), which is valid for vertical barriers.

Finally, the simulations carried out have confirmed that passive barriers can reduce the hazardous distance when their size exceeds a given threshold. Such a threshold can be estimated accordingly with a criterion previously developed for foreseeing when an obstacle influences significantly the hazardous cloud dispersion (Derudi, et al., 2014), as can be deduced from the results summarized in Figure 6A.

6 Conclusions

The aim of this work was to analyze the influence of active barriers on the mitigation of a dense cloud arising from an accidental loss of LNG. Passive barriers are very simple mitigation methods that consist of a wall that physically hinders the cloud advancement. Active barriers involve curtains added to the passive barriers which introduce further dilution due to the transfer of momentum from the curtain to the cloud and the entrainment of air from the environment.
It was found that active barriers can reduce the hazardous distance following an accidental release of LNG more effectively than passive barriers.

In particular, the jet located on the top of the barrier acts both as a physical barrier by stopping cloud advancement, and as a driving force for diluting the cloud thanks to the jet entrainment from the cloud and the air side. These two effects, which are almost independent of the kind and the temperature of the jet, improve the efficiency of the mitigation barriers, giving a lower hazardous distance with respect to passive barriers of the same height. However, this also means that active barriers can achieve the same performances as passive barrier with a lower height.
A rule-of-thumb was proposed for a rough estimation of the jet velocity required when using vertical jets, and its validity was confirmed by CFD simulations. Moreover, it was also shown that by using an active mitigation barrier with the top tilted upwind by about 45°, it is possible to reduce the jet velocity (and therefore the required air flow rate) by about one half.
Two case studies were investigated to highlight the potentialities and limitations of the proposed procedure for designing active mitigation barriers.
The first case study involved the full-bore rupture of an LNG pipeline leading to a massive release of dense gas. In this case, a 6 m high tilted active mitigation barrier with an air flow rate of about 1000 Nm^3/s lasting for about 300 s is required to stop cloud dispersion: this would require the storage of about $3 \cdot 10^5$ Nm^3 of pressurized air ready for prompt intervention in case of accidents. Using commercial vessels of 2.5 m^3 at 400 bar and with a height of 12 m would result in about 300 cylinders, which could be assembled in a cubic framework of 8x8x12 m^3. However, it should be noted that the calculated failure per year of operation rate, based on pipe length, established by FERC (Federal Energy Regulatory Commission) and adopted by PHMSA (Pipeline and Hazardous Materials Safety Administration) for a catastrophic rupture of a 1 m pipeline is in the order of 10^{-7}-10^{-8}, which is lower than the $3 \cdot 10^{-5}$ Failure Rate Criterion, therefore the event does not require the evaluation of accidental flow.
The second case study, which represents a more realistic scenario, involved the leakage of LNG from a pipeline leading to a more contained release of the dense gas. In this case, the 6 m high tilted active mitigation barrier would require an air flow rate of about 400 Nm^3/s lasting for about 300 s: this would lead to the storage of about $1.2 \cdot 10^5$ Nm^3 of pressurized air ready for a prompt intervention in case of accidents. Using commercial vessels of 2.5 m^3 at 400 bar, a height of 12 m would result in about 120 cylinders, which could be arranged in a cubic framework of 5x5x12 m^3.

References

ANSYS Inc. (2004). *GAMBIT 2.2 Tutorial Guide*. Lebanon, NH, USA.

ANSYS Inc. (2009). ANSYS Fluent 12 User's guide. Lebanon, NH, USA.

Awbi, H. B. (1991). *Ventilation of buildings*: E & FN Spon.

Bara, A., & Dusserre, G. (1997). The use of water curtains to protect firemen in case of heavy gas dispersion. *Journal of Loss Prevention in the Process Industries, 10*(3), 179-183. doi: http://dx.doi.org/10.1016/S0950-4230(96)00049-6

Blocken, B., van der Hout, A., Dekker, J., & Weiler, O. (2015). CFD simulation of wind flow over natural complex terrain: Case study with validation by field measurements for Ria de Ferrol, Galicia, Spain. *Journal of Wind Engineering and Industrial Aerodynamics, 147*, 43-57. doi: 10.1016/j.jweia.2015.09.007

Britter, R. E., & Griffiths, R. F. (1982). The role of dense gases in the assessment of industrial hazards. *Journal of Hazardous Materials, 6*(1–2), 3-12. doi: http://dx.doi.org/10.1016/0304-3894(82)80032-0

Buchlin, J.-M. (1994). Mitigation of problem clouds. *Journal of Loss Prevention in the Process Industries, 7*(2), 167-174. doi: http://dx.doi.org/10.1016/0950-4230(94)80035-9

Busini, V., Lino, M., & Rota, R. (2012). Influence of Large Obstacles and Mitigation Barriers on Heavy Gas Cloud Dispersion: a Liquefied Natural Gas Case-Study. *Industrial & Engineering Chemistry Research, 51*(22), 7643-7650. doi: 10.1021/Ie201591b

Busini, V., & Rota, R. (2014). Influence of the shape of mitigation barriers on heavy gas dispersion. *Journal of Loss Prevention in the Process Industries, 29*, 13-21. doi: 10.1016/j.jlp.2014.01.001

Derudi, M., Bovolenta, D., Busini, V., & Rota, R. (2014). Heavy Gas Dispersion in Presence of Large Obstacles: Selection of Modeling Tools. *Industrial & Engineering Chemistry Research, 53*(22), 9303-9310. doi: 10.1021/ie4034895

Diaz-Ovalle, C., Vazquez-Roman, R., Lesso-Arroyo, R., & Mannan, M. S. (2012). A simplified steady-state model for air, water and steam curtains. *Journal of Loss Prevention in the Process Industries, 25*(6), 974-981. doi: http://dx.doi.org/10.1016/j.jlp.2012.05.011

DNV. (1999). PHAST 6.0 Technical Reference Manual. London, UK.

Ermak, D. L., Chan, S. T., Morgan, D. L., & Morris, L. K. (1982). A comparison of dense gas dispersion model simulations with burro series LNG spill test results. *Journal of Hazardous Materials, 6*(1–2), 129-160. doi: http://dx.doi.org/10.1016/0304-3894(82)80037-X

Kim, B. K., Mentzer, R. A., & Mannan, M. S. (2014). Numerical Study on Physical Mechanisms of Forced Dispersion for an Effective LNG Spill Mitigation. *Industrial & Engineering Chemistry Research, 53*(22), 9488-9498. doi: 10.1021/ie400738p

Koopman, R. P., Cederwall, R. T., Ermak, D. L., Goldwire Jr, H. C., Hogan, W. J., McClure, J. W., . . . Shinn, J. H. (1982). Analysis of Burro series 40-m3 lng spill experiments. *Journal of Hazardous Materials, 6*(1–2), 43-83. doi: http://dx.doi.org/10.1016/0304-3894(82)80034-4

Koopman, R. P., & Ermak, D. L. (2007). Lessons learned from LNG safety research. *Journal of Hazardous Materials, 140*(3), 412-428. doi: 10.1016/j.jhazmat.2006.10.042

Koopman, R. P., Ermak, D. L., & Chan, S. T. (1989). A Review of Recent Field-Tests and Mathematical-Modeling of Atmospheric Dispersion of Large Spills of Denser-Than-Air Gases. *Atmospheric Environment, 23*(4), 731-745. doi: 10.1016/0004-6981(89)90475-7

Luketa-Hanlin, A. (2006). A review of large-scale LNG spills: Experiments and modeling. *Journal of Hazardous Materials, 132*(2-3), 119-140. doi: 10.1016/j.jhazmat.2005.10.008

Luketa-Hanlin, A., Koopman, R. P., & Ermak, D. L. (2007). On the application of computational fluid dynamics codes for liquefied natural gas dispersion. *Journal of Hazardous Materials, 140*(3), 504-517. doi: 10.1016/j.jhazmat.2006.10.023

Pontiggia, M., Derudi, M., Busini, V., & Rota, R. (2009). Hazardous gas dispersion: A CFD model accounting for atmospheric stability classes. *Journal of Hazardous Materials, 171*(1-3), 739-747. doi: 10.1016/j.jhazmat.2009.06.064

Puttock, J. S., Blackmore, D. R., & Colenbrander, G. W. (1982). Field experiments on dense gas dispersion. *Journal of Hazardous Materials, 6*(1–2), 13-41. doi: http://dx.doi.org/10.1016/0304-3894(82)80033-2

Rajaratnam, N. (1976). *Turbulent jets*. Amsterdam: Elsevier.

Rana, M. A., Cormier, B. R., Suardin, J. A., Mang, Y. C., & Mannan, M. S. (2008). Experimental Study of Effective Water Spray Curtain Application in Dispersing Liquefied Natural Gas Vapor Clouds. *Process Safety Progress, 27*(4), 345-353. doi: 10.1002/prs.10275

Rana, M. A., Guo, Y. Y., & Mannan, M. S. (2010). Use of water spray curtain to disperse LNG vapor clouds. *Journal of Loss Prevention in the Process Industries, 23*(1), 77-88. doi: 10.1016/j.jlp.2009.06.003

Schleder, A. M., Pastor, E., Planas, E., & Martins, M. R. (2015). Experimental data and CFD performance for cloud dispersion analysis: The USP-UPC project. *Journal of Loss Prevention in the Process Industries, 38*, 125-138. doi: 10.1016/j.jlp.2015.09.003

Zhang, X., Li, J., Zhu, J., & Qiu, L. (2015). Computational fluid dynamics study on liquefied natural gas dispersion with phase change of water. *International Journal of Heat and Mass Transfer, 91*, 347-354. doi: 10.1016/j.ijheatmasstransfer.2015.07.117